Rapid Communications

Controlling the deformation of metamaterials: Corner modes via topology

Adrien Saremi and Zeb Rocklin
School of Physics, Georgia Institute of Technology, Atlanta, Georgia 30332, USA

(Received 20 April 2018; published 29 November 2018)

Topological metamaterials have invaded the mechanical world, demonstrating acoustic cloaking and waveguiding at finite frequencies and variable, tunable elastic response at zero frequency. Zero-frequency topological states have previously relied on the Maxwell condition, namely, that the system has equal numbers of degrees of freedom and constraints. Here, we show that otherwise rigid periodic mechanical structures are described by a map with a nontrivial topological degree (a generalization of the winding number introduced by Kane and Lubensky) that creates, directs, and protects modes on their boundaries. We introduce a model system consisting of rigid quadrilaterals connected via free hinges at their corners in a checkerboard pattern. This bulk structure generates a topological linear deformation mode exponentially localized in one corner, as investigated numerically and via an experimental prototype. Unlike the Maxwell lattices, these structures select a single desired mode, which controls variable stiffness and mechanical amplification that can be incorporated into devices at any scale.

DOI: 10.1103/PhysRevB.98.180102

I. INTRODUCTION

Topological phases of matter have been realized most famously in electronic systems [1–6], but also in classical ones consisting of active fluids [7–10], air flows [11–13], photons [14–16], vibrating mechanical elements [17–19], and spinning gyroscopes [20–22]. Across this vast range of systems, the topological paradigm (1) identifies various invariants that assume discrete values determined by the bulk structure that (2) are insensitive to continuous deformations and (3) determines protected edge modes. We consider yet another class of topological systems, zero-frequency mechanical ones, that has been shown to have a topological invariant protected by the Maxwell condition, that the system's degrees of freedom (DOF) and constraints are equal in number, and that determines the placement of topological modes on open boundaries and interfaces [23], point defects [24], and even the bulk [25]. Such systems have been demonstrated or proposed as new ways of controlling origami and kirigami folding [26], beam buckling [27] and fracture [28], as well as composing nonreciprocal mechanical diodes [29] and mechanically programmable materials [24]. Acoustic systems, although fundamentally distinct from lattice systems in being continuous, are alike in supporting topological states, resulting in wave propagation that is backscattering free [17,18,30] and, when time-reversal symmetry is broken, unidirectional [11,20–22,31], permitting unprecedented waveguiding and cloaking capabilities.

As well as such examples of topological modes one dimension lower than the bulk, exciting new predictions have been made concerning higher-order topological modes on lower-dimensional surface elements, such as those split between the four corners of a square two-dimensional (2D) system [32–36]. Such modes, subsequently observed in a phononic system [37] and a microwave circuit system [38] with mirror symmetries, raise the possibility of higher-order mechanical modes. Here, we report just such a family of topological lattices, presenting both a general theory and a detailed and experimentally realized example: the 2D "deformed checkerboard" lattice. These lattices possess higher-order mechanical criticality, in the sense of having modes localized to lower-dimensional sections of their boundaries. In contrast with the many boundary modes of Maxwell lattices, isolated zero modes are present in otherwise *rigid* materials (and the force-bearing self-stresses in otherwise floppy ones), amounting to a fundamentally new and topologically nontrivial capability among flexible mechanical metamaterials [39].

II. HIGHER-ORDER MAXWELL RIGIDITY

A. A new counting argument

Consider a system governed by a *constraint matrix* $\mathbf{C}$ which linearly maps some coordinates $\mathbf{u}$ (often displacements of sites) to another vector $\mathbf{e}$ (often extensions of stiff mechanical elements). Modes $\mathbf{e}$ in the null space of $\mathbf{C}^{\mathrm{T}}$ are called *self-stresses*, (generalized) tensions that do not generate force. Because of this relation, the rank-nullity relation of linear algebra implies

$$N_{\mathrm{zm}} - N_{\mathrm{ss}} = N_{\mathrm{DOF}} - N_{\mathrm{con}}, \tag{1}$$

where the four symbols refer respectively to the system's numbers of zero modes, self-stresses, degrees of freedom, and constraints. This equality is, in the context of constraint matrices of ball and spring systems, owed to Calladine [40], Maxwell a century earlier noting the phenomenon of redundant constraints, but not identifying self-stresses [41]. We consider a generalized notion of constraints leading to generalized pseudoforces.

For periodic systems in d dimensions, this can be further refined by assuming that the displacements within a single cell indexed by $\mathbf{n} = (n_1, n_2, \ldots, n_d)$ are of the "z-periodic"

form $\mathbf{u_n} = \mathbf{u}\prod_i z_i^{n_i}$, where z_i is a complex number of any magnitude, as used in surface quantum wave functions [42–44]. Indeed, due to an argument similar to Bloch's theorem, any normal mode of a system with a periodic bulk must have such a form. $\mathbf{u}$ thus plays the role of the wave function: a complex vector describing a state in a periodic system whose overall magnitude and phase do not matter with a functional dependence on the (complex) wave vector. For a finite system with open boundary conditions, a mode with, e.g., $|z_1| < 1$ exists exponentially localized on the left-hand boundary. Kane and Lubensky exploited this index theorem in *Maxwell* systems (those with $n_{\mathrm{DOF}} = n_{\mathrm{con}}$), to relate the number of such zero modes, for which $\det[\mathbf{C}(\mathbf{z})] = 0$, to the winding of the phase of $\det[\mathbf{C}(\mathbf{z})]$ as z_1 winds around the bulk ($z_1 = e^{i\theta_1}$) [23]. Physically, such modes are any change in system configuration (movements of particles, changes in electrical currents, rotations of spins, etc.) that satisfy the linear constraints. As we now present, the one-dimensional winding number is only one example of a whole family of topological invariants.

The Maxwell condition is a mechanical critical condition [45] which identifies systems expected to have boundary modes from missing bonds at boundaries. More generally, rather than fixing some intercell evolution via $\mathbf{z}$, we can vary n of the z_i ($n \leqslant d$) as well as $\mathbf{u}$, the shape of the mode within a single cell, generating n additional "degrees of freedom." Thus, upon normalizing our linear mode, the configuration space has dimension $n + n_{\mathrm{DOF}} - 1$, and zero modes require satisfying n_{con} constraint conditions. Thus, the critical condition under which we would expect (for compatible and independent constraints) isolated zero modes on a surface element n dimensions lower than the system's bulk is

$$n = n_{\mathrm{con}} + 1 - n_{\mathrm{DOF}}. \tag{2}$$

For the case of $n = 1$, this is simply Maxwell rigidity; more generally, we refer to it as nth-*order Maxwell rigidity*. For $n = 1$, the constraint matrix resembles a non-Hermitian but square Hamiltonian, known to possess nontrivial topology [46–55], whereas for higher-order systems the constraint map connects spaces of modes and constraints that are different sizes. For the present work we shall focus on the case $d = 2$, $n = 2$, in which zero modes are exponentially localized in corners. In 3D, one can have corner (third-order) *or* edge modes (second-order rigidity), as indicated in Fig. 1. Because of the duality between the rigidity and equilibrium matrices, it is also possible to have higher-order self-stresses in *underconstrained* systems, below the Maxwell point, satisfying $n = n_{\mathrm{DOF}} + 1 - n_{\mathrm{con}}$. Bulk zero modes are always compatible with free boundary conditions; bulk self-stresses are permitted by fixed boundaries.

B. Higher-order topological invariant

The topological paradigm is to relate the existence of boundary modes to bulk structure. We now describe how to relate the presence of the topological modes on our $(d-n)$-dimensional surface element to the topological degree of a map over the surrounding $(d-n+1)$-dimensional elements (e.g., a corner mode via the two adjoining edges).

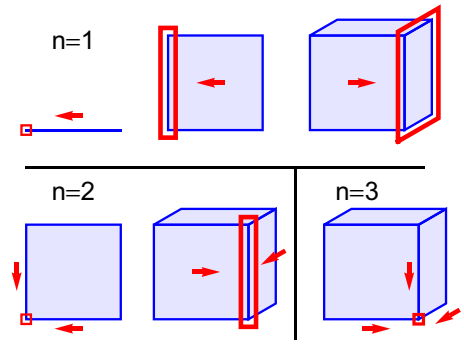

FIG. 1. Systems at the conventional ($n = 1$ Maxwell critical point acquire zero modes (red) from missing bonds at open boundaries. Imbalances in these modes result from topological polarization (arrows) of the system's d-dimensional bulk. Systems with higher-order $n > 1$ Maxwell rigidity have polarized surface elements, resulting in modes in corners and (in $d = 3$) along 1D edges, defying conventional constraint counting.

Let us describe a region $\mathcal{B}$ of configuration space in which modes have amplitude $\mathbf{u}^2 = 1$ and $0 \leqslant |z_i| \leqslant 1$, $i = 1, 2, \ldots, n$ and are thus exponentially localized to the surface element in question. Consider then the nonlinear but continuous polynomial (or, in a more general gauge, Laurent polynomial) map from $\mathcal{B}$ to the constraints $\mathbf{e} = \mathbf{C}(\mathbf{z})\mathbf{u}$. Given the criticality condition of Eq. (2), these spaces have the same dimension, and $J_C(\mathbf{v})$, the Jacobian determinant of this map, gives the signed ratio of their volume elements as a function of the vector coordinate $\mathbf{v}$. As discussed in the Supplemental Material [56], the number of zeros in $\mathcal{B}$ can then be determined by evaluating the number of times $\partial\mathcal{B}$'s map to the normalized constraint space $\hat{e} = \mathbf{e}/|\mathbf{e}|$ covers the real unit sphere $S^{2n_{\mathrm{con}}-1}$,

$$N_{\mathcal{B}} = A^{-1}_{2n_{\mathrm{con}}-1}\int_{\partial\mathcal{B}} dv_1 \cdots dv_{2n_{\mathrm{con}}-1} J_C(\mathbf{v}). \tag{3}$$

Here, A_j is the surface area of the j-dimensional hypersphere. This topological map then relates the presence of zero modes in nth-order critical systems to nonlinear maps from modes to constraints on the surrounding elements, such as the three edges adjoining the corner of a cube, generalizing the first-order topological invariant of Kane and Lubensky, a winding number that relates bulk structure to surface modes [23]. In the context of bulk-edge correspondence, a corner functions as the edge of the edges or even the interface between edges, in that its topological modes are protected by the invariant integrated over the edge modes. It does, however, depend on the entire bulk insofar as that it determines the form of the constraint map. Although the homotopy group of maps of spheres to themselves is integers [$\pi_n(S^n) = \mathbb{Z}$], our holomorphic maps always have non-negative degrees corresponding to the number of modes enclosed.

C. Polarization of general surface elements

We now discuss the mechanical polarization of structural elements. Consider a system with isolated zero modes, or zero modes which are isolated once transverse wave vectors are fixed (e.g., a 2D Maxwell structure has polarization which depends on a transverse wave vector [25]). One of its surface

elements possesses a number of zero modes, which we refer to as its *charge*, continuing terminology used in mechanics to describe not only topology [23,24] but also purely geometrical singularities [57]. Equation (3) may be used to obtain this charge: For example, the charge on corners of a 2D second-order critical lattice is

$$N_{\sigma_1,\sigma_2} = \int_{-1}^{1} dv_0 \int_{-\pi}^{\pi} dv_1 \int_{-\pi}^{\pi} dv_2 \, J_C^{\sigma_1,\sigma_2}(\mathbf{v}), \qquad (4)$$

where the arguments of the Jacobian describe real coordinates over values $z_i = r_i e^{i\theta_i}$ and, more generally, the mode shape $\mathbf{u}$. Since these are modes that bound the corner modes, they lie on the adjoining edges. To obtain in this manner the charge on, e.g., the upper left corner ($\sigma_1 = -$, $\sigma_2 = +$), coordinates must be chosen to compactify the space and gauge must be chosen to maintain a holomorphic map as described in the Supplemental Material [56].

From these charges we may define the polarizations of all elements of the structure. For example, the second-order 2D structure has, in our language, polarizations of its bulk given by differences between charges of opposing edges and polarizations of its edges given by differences in corner charges.

This reveals nontrivial relationships between the charges and polarizations of various elements. The edge polarizations, along with the overall charge of the structure, suffice to determine the corner charges. However, the edge charges (or, alternately, the bulk dipole polarization) cannot determine the same without a topological quadrupole charge $q = N_{++} + N_{--} - (N_{-+} + N_{+-})$ of the type described in higher-order electronics [32–36] and phononics [37]. Despite this intriguing connection, the present corner mode is clearly distinct from those quadrupole modes in that it occurs at zero frequency and does not require any mirror symmetries. Indeed, it applies even to systems with irregular boundaries.

While 0D corners necessarily have integer numbers of modes, 1D edges of 3D structures with second-order Maxwell rigidity may have a fractional charge. Such a situation was observed in 2D [25,58] and 3D [59] for Maxwell lattices (those with $n_{\mathrm{con}} = n_{\mathrm{DOF}}$). In our higher-order analog, we would expect the face between two fractionally charged edges to host a sinusoidal zero-energy deformation.

III. MODEL SECOND-ORDER SYSTEM: THE DEFORMED CHECKERBOARD

To model the general phenomenon of higher-order Maxwell rigidity, we consider the simplest case, second-order rigidity in 2D, which occurs in lattices with one additional constraint per cell beyond the Maxwell condition [Eq. (2)]. Our chosen system is the deformed checkerboard, consisting of rigid quadrilaterals joined at free hinges as shown in Fig. 2, which can be thought of as the result of fusing two triangles together in the deformed kagome lattice [23] or rigidifying an open quadrilateral in the deformed square lattice [25]. As shown in the Supplemental Material [56], any zero-energy deformation of this system may be described by the scalar shearing of the voids between pieces of the form $s_{n_1,n_2} = s_0 z_1^{n_1} z_2^{n_2}$. Each void's shearing is coupled to that of its four neighbors by their shared vertices, resulting in the

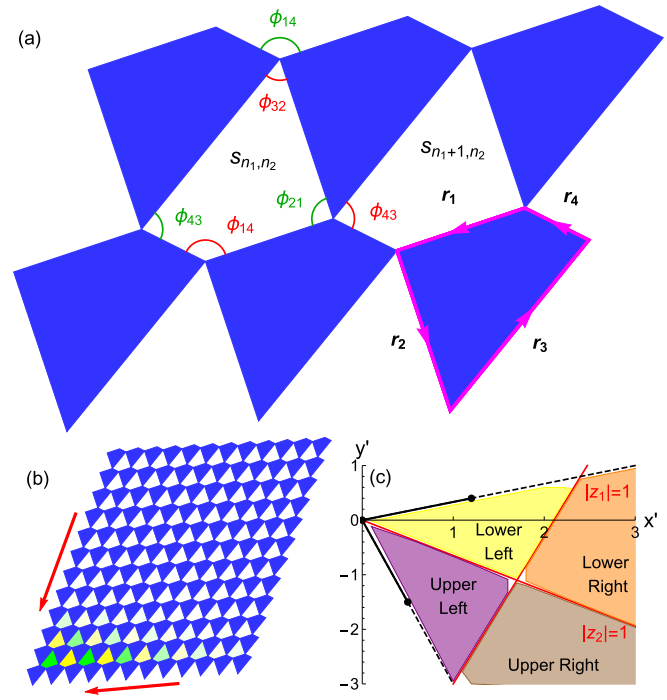

FIG. 2. (a) Solid pieces in the system are hinged and allowed to rotate relative to one another. A given void between pieces can shear, but this motion is coupled to that of four of its neighbors, leading to an overconstrained system. (b) The unique zero-energy deformation is exponentially localized in one of four corners, with green and yellow shading indicating shearing in opposite directions. This topological mode lies between two topologically polarized edges (red arrows). (c) In a two-dimensional region of parameter space in which three of the piece's vertices are fixed and the fourth is placed at (x', y'), the location of the corner mode is in agreement with the numerically obtained topological degree of the map (shading).

overconstrained constraint matrix

$$\mathbf{C}(z_1, z_2) = \begin{pmatrix} b_1 + a_1 z_1 \\ b_2 + a_2 z_2 \end{pmatrix}. \qquad (5)$$

As is now clear, the unique zero-energy deformation has $z_i = -b_i/a_i < 0$, where the relative magnitudes of $a_i, b_i > 0$ determine in which corner it is exponentially localized. This mode is antiferromagnetic, in the sense that each piece rotates in the opposite direction from its four neighbors (also translating slightly). This form reveals an important effect of symmetry: When $a_i = b_i$ and the constraint matrix is therefore invariant under the reflection $n_i \to -n_i$, the mode lies on an edge rather than a corner. However, this symmetry is evident only in Eq. (5)—it corresponds to quadrilateral pieces that are not themselves symmetric but whose centers of mass lie on the lines connecting their opposing vertices. It is only when both such conditions are met, with parallelogram pieces, that the mode enters the bulk and extends to a nonlinear mechanism. Indeed, by evolving the system through the parameter space shown in Fig. 2(c) (which would require altering the shape of the piece) around this parallelogram point, one could "pump" the mode from corner to corner around the structure.

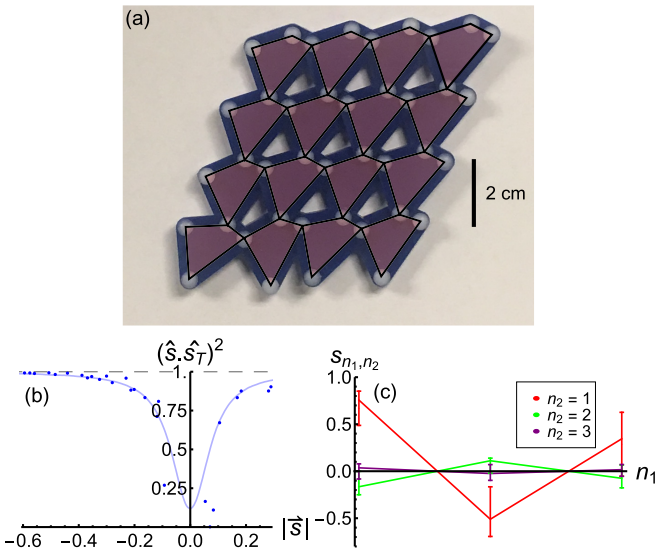

FIG. 3. (a) A hinged prototype of the checkerboard lattice. (b) $\vec{s}$ describes the change in the relative angles of pieces, measured in radians; $(\hat{s} \cdot \hat{s}_T)^2 = 1$ corresponds to an observed mode entirely predicted by the topological mode. Over a broad range of amplitudes, the topological component $\hat{s}_T$ is the dominant mode present. (c) Configurations in cells indexed by (n_1, n_2), indicated by error bars, are in agreement with theory lines.

A. Experimental realization

We realize the topological metamaterial by using a high-precision programmable laser cutter (Trotec Speedy 300) to cut ∼1-cm pieces from 3.2-mm-thick acrylic sheets. Nylon rivets are placed through snug holes in the pieces to join them at freely rotating hinges, with a 4×4 prototype then assembled, as shown in Fig. 3(a). The prototype is rigid throughout the bulk and most of the boundary, with a zero mode consisting of counter-rotating rigid pieces localized in the corner predicted by the constraints of Eq. (5), as shown in the video in the Supplemental Material [56]. This easily realized prototype permits the testing of the practical effects of friction, static disorder, and geometrical nonlinearities on our idealized theory. These limitations prevent the system from acting as an exponential mechanical amplifier (as was recently treated at certain edges of disordered systems near the first-order Maxwell point [60]) though some amplification in deformation is observed when the prototype is manipulated near the charged corner.

A digital camera is used to track the centers of the rivets as the system is deformed. Despite the linear nature of the theory, the compressibility of the rivets allows a $(-0.43, 0.31)$ rad range (in the most-deformed void) of configurations in which static friction leaves the prototype stable without any external support. The vector of shears for the nine voids $\vec{s}$ was tracked across this range, and compared to the predicted topological mode $\hat{s}_T$. The topological character is plotted as a function of mode amplitude in Fig. 3(b). The numerical prediction shown assumes a topological mode and independent normally distributed errors throughout the system. As shown in Fig. 3(c), the topological mode is dominant everywhere save where its amplitude is lowest and static friction most relevant.

Thus, we have shown that even in real, easily realized systems possessing disorder, nonlinearities, and friction, the topological mode appears as predicted and accounts for a broad range of mechanical responses. 3D printing has already achieved 3D Maxwell systems [61], though a challenge remains in creating "hinged" pieces that rotate much more easily than they deform. Unlike 2D Maxwell lattices, which require careful control of the boundary because of the many deformation modes [62], our system is mechanically stable because it has only a single, linear mechanism.

IV. DISCUSSION

We have described a family of higher-order topological invariants that describes a class of periodic mechanical systems with zero-frequency boundary modes. These modes are protected not by symmetries but by a new index theorem relating the number of degrees of freedom and constraints to the dimensions of the bulk and boundary [Eq. (2)]. They are generated, protected, and placed on particular surface elements by the topological degree of the constraint map [Eq. (3)], making an association in full generality with the physical modes. In particular, we have experimentally realized a two-dimensional structure with a single mode and demonstrated its mechanical response. The existence of the mode is protected by the index theorem, and its placement in a desired corner determined by a topological covering number, with further fine tuning possible through geometric distortions. This allows for a material such as is realizable with 3D printing techniques [61] with a unique programed mode, topologically protected by its bulk structure.

This paradigm relies on the structure's periodicity and on particular boundary conditions, but is not limited to mechanical zero modes. Indeed, a Maxwell-Cremona dual [63,64], in which a mechanical network's vertices and faces exchange roles, exists for the deformed checkerboard with a topological corner self-stress. More generally, nonmechanical systems with varying numbers of constraints and degrees of freedom, such as spin systems [65], electrical circuits [66–68], and others, can have topological boundary modes protected by the index theorem and winding numbers.

Our systems lie at the intersection of two exciting areas of research. One is into the finite-frequency higher-order modes mentioned in Sec. I, compared and contrasted with the present case in Sec. III. The other, Maxwell lattices with Kane-Lubensky topological polarization, fall within our paradigm as systems with balanced numbers of degrees of freedom with boundary modes one dimension lower than their bulk. The original Maxwell index theorem [Eq. (1)] offers the advantage that the Maxwell modes extend nonlinearly, and exist despite disorder. In contrast, our more general modes are only linear (barring an additional symmetry, such as parallelogram tiles in the deformed checkerboard) and rely on perfect periodicity, though as our prototype demonstrates, it is still easy to realize the topological mode under realistic conditions. And such modes have the advantage that the rest of the structure is rigid, and that the modes are unique, rather than being part of a family that mixes nonlinearly in ways that are difficult to control [62].

The topological connection between bulk and boundary, constraints, and degrees of freedom presents a number of immediate avenues for further study. Three-dimensional systems, which have already demonstrated unique features in Maxwell systems [59], should admit not only the 2D face modes of that study and the 0D corner modes corresponding to this one, but intermediate 1D edge (hinge) modes. Other systems, such as origami and kirigami [26], have mixed dimension (a 2D sheet embedded in 3D space) or simply more intricate constraints [69]. Finally, one may think of boundaries as a particular case of defects of given dimension, making contact with the extensive categorization of defects in topological insulators [4], admitting the same possibility of defect engineering observed in topological Maxwell lattices [24]. Because of our map's nonlinearity, it may shed light on nonlinear excitations of polarized lattices [70].

Note added. Recently, a systematic study of constraint matrices with a broader range of dimensions and symmetries was posted [71], situating the integer invariant considered here in a large, exciting array of topological states.

ACKNOWLEDGMENTS

The authors gratefully acknowledge helpful conversations with Bryan G. Chen, Michael Lawler, Tom Lubensky, Xiaoming Mao, Massimo Ruzzene, Christian Santangelo, and Vincenzo Vitelli.

[1] D. J. Thouless, M. Kohmoto, M. P. Nightingale, and M. den Nijs, Phys. Rev. Lett. **49**, 405 (1982).
[2] C. L. Kane and E. J. Mele, Phys. Rev. Lett. **95**, 226801 (2005).
[3] B. A. Bernevig, T. L. Hughes, and S.-C. Zhang, Science **314**, 1757 (2006).
[4] J. C. Y. Teo and C. L. Kane, Phys. Rev. B **82**, 115120 (2010).
[5] M. Z. Hasan and C. L. Kane, Rev. Mod. Phys. **82**, 3045 (2010).
[6] X.-L. Qi and S.-C. Zhang, Rev. Mod. Phys. **83**, 1057 (2011).
[7] B. C. van Zuiden, J. Paulose, W. T. Irvine, D. Bartolo, and V. Vitelli, Proc. Natl. Acad. Sci. U.S.A. **113**, 12919 (2016).
[8] A. Souslov, B. C. van Zuiden, D. Bartolo, and V. Vitelli, Nat. Phys. **13**, 1091 (2017).
[9] A. Murugan and S. Vaikuntanathan, Nat. Commun. **8**, 13881 (2017).
[10] K. Dasbiswas, K. K. Mandadapu, and S. Vaikuntanathan, Proc. Natl. Acad. Sci. U.S.A. **115**, E9031 (2018).
[11] A. B. Khanikaev, R. Fleury, S. H. Mousavi, and A. Alù, Nat. Commun. **6**, 8260 (2015).
[12] C. He, X. Ni, H. Ge, X.-C. Sun, Y.-B. Chen, M.-H. Lu, X.-P. Liu, and Y.-F. Chen, Nat. Phys. **12**, 1124 (2016).
[13] Z.-G. Chen and Y. Wu, Phys. Rev. Appl. **5**, 054021 (2016).
[14] M. C. Rechtsman, J. M. Zeuner, Y. Plotnik, Y. Lumer, D. Podolsky, F. Dreisow, S. Nolte, M. Segev, and A. Szameit, Nature (London) **496**, 196 (2013).
[15] L. Lu, J. D. Joannopoulos, and M. Soljačić, Nat. Photonics **8**, 821 (2014).
[16] V. Peano, C. Brendel, M. Schmidt, and F. Marquardt, Phys. Rev. X **5**, 031011 (2015).
[17] R. Süsstrunk and S. D. Huber, Science **349**, 47 (2015).
[18] J. Vila, R. K. Pal, and M. Ruzzene, Phys. Rev. B **96**, 134307 (2017).
[19] G. Trainiti, J. Rimoli, and M. Ruzzene, J. Appl. Phys. **123**, 091706 (2018).
[20] L. M. Nash, D. Kleckner, A. Read, V. Vitelli, A. M. Turner, and W. T. Irvine, Proc. Natl. Acad. Sci. U.S.A. **112**, 14495 (2015).
[21] P. Wang, L. Lu, and K. Bertoldi, Phys. Rev. Lett. **115**, 104302 (2015).
[22] N. P. Mitchell, L. M. Nash, D. Hexner, A. M. Turner, and W. T. Irvine, Nat. Phys. **14**, 380 (2018).
[23] C. Kane and T. Lubensky, Nat. Phys. **10**, 39 (2014).
[24] J. Paulose, B. G.-g. Chen, and V. Vitelli, Nat. Phys. **11**, 153 (2015).
[25] D. Z. Rocklin, B. G.-g. Chen, M. Falk, V. Vitelli, and T. C. Lubensky, Phys. Rev. Lett. **116**, 135503 (2016).
[26] B. G.-g. Chen, B. Liu, A. A. Evans, J. Paulose, I. Cohen, V. Vitelli, and C. D. Santangelo, Phys. Rev. Lett. **116**, 135501 (2016).
[27] J. Paulose, A. S. Meeussen, and V. Vitelli, Proc. Natl. Acad. Sci. U.S.A. **112**, 7639 (2015).
[28] L. Zhang and X. Mao, New J. Phys. **20**, 063034 (2018).
[29] C. Coulais, D. Sounas, and A. Alù, Nature (London) **542**, 461 (2017).
[30] R. K. Pal, M. Schaeffer, and M. Ruzzene, J. Appl. Phys. **119**, 084305 (2016).
[31] Y.-T. Wang, P.-G. Luan, and S. Zhang, New J. Phys. **17**, 073031 (2015).
[32] W. A. Benalcazar, B. A. Bernevig, and T. L. Hughes, Science **357**, 61 (2017).
[33] W. A. Benalcazar, B. A. Bernevig, and T. L. Hughes, Phys. Rev. B **96**, 245115 (2017)
[34] Z. Song, Z. Fang, and C. Fang, Phys. Rev. Lett. **119**, 246402 (2017).
[35] J. Langbehn, Y. Peng, L. Trifunovic, F. von Oppen, and P. W. Brouwer, Phys. Rev. Lett. **119**, 246401 (2017).
[36] F. Schindler, A. M. Cook, M. G. Vergniory, Z. Wang, S. S. Parkin, B. A. Bernevig, and T. Neupert, Sci. Adv. **4**, eaat0346 (2018).
[37] M. Serra-Garcia, V. Peri, R. Süsstrunk, O. R. Bilal, T. Larsen, L. G. Villanueva, and S. D. Huber, Nature (London) **555**, 342 (2018).
[38] C. W. Peterson, W. A. Benalcazar, T. L. Hughes, and G. Bahl, Nature (London) **555**, 346 (2018).
[39] K. Bertoldi, V. Vitelli, J. Christensen, and M. van Hecke, Nat. Rev. Mater. **2**, 17066 (2017).
[40] C. Calladine, Int. J. Solids Struct. **14**, 161 (1978).
[41] J. C. Maxwell, London, Edinburgh Dublin Philos. Mag. J. Sci. **27**, 294 (1864).
[42] A. Alase, E. Cobanera, G. Ortiz, and L. Viola, Phys. Rev. Lett. **117**, 076804 (2016).
[43] A. Alase, E. Cobanera, G. Ortiz, and L. Viola, Phys. Rev. B **96**, 195133 (2017).
[44] E. Cobanera, A. Alase, G. Ortiz, and L. Viola, J. Phys. A: Math. Theor. **50**, 195204 (2017).
[45] T. Lubensky, C. Kane, X. Mao, A. Souslov, and K. Sun, Rep. Prog. Phys. **78**, 073901 (2015).

[46] K. Esaki, M. Sato, K. Hasebe, and M. Kohmoto, Phys. Rev. B **84**, 205128 (2011).
[47] S.-D. Liang and G.-Y. Huang, Phys. Rev. A **87**, 012118 (2013).
[48] T. E. Lee, Phys. Rev. Lett. **116**, 133903 (2016).
[49] D. Leykam, K. Y. Bliokh, C. Huang, Y. D. Chong, and F. Nori, Phys. Rev. Lett. **118**, 040401 (2017).
[50] H. Menke and M. M. Hirschmann, Phys. Rev. B **95**, 174506 (2017).
[51] Y. Xu, S.-T. Wang, and L.-M. Duan, Phys. Rev. Lett. **118**, 045701 (2017).
[52] J. González and R. A. Molina, Phys. Rev. B **96**, 045437 (2017).
[53] W. Hu, H. Wang, P. P. Shum, and Y. D. Chong, Phys. Rev. B **95**, 184306 (2017).
[54] Y. Xiong, J. Phys. Commun. **2**, 035043 (2018).
[55] H. Shen, B. Zhen, and L. Fu, Phys. Rev. Lett. **120**, 146402 (2018).
[56] See Supplemental Material at http://link.aps.org/supplemental/10.1103/PhysRevB.98.180102 for further details, which includes a video and Refs. [72,73].
[57] M. Moshe, E. Esposito, S. Shankar, B. Bircan, I. Cohen, D. R. Nelson, and M. J. Bowick, arXiv:1801.08263.
[58] H. C. Po, Y. Bahri, and A. Vishwanath, Phys. Rev. B **93**, 205158 (2016).
[59] G. Baardink, A. Souslov, J. Paulose, and V. Vitelli, Proc. Natl. Acad. Sci. U.S.A. **115**, 489 (2018).
[60] L. Yan, J.-P. Bouchaud, and M. Wyart, Soft Matter **13**, 5795 (2017).
[61] O. R. Bilal, R. Süsstrunk, C. Daraio, and S. D. Huber, Adv. Mater. **29**, 1700540 (2017).
[62] D. Z. Rocklin, S. Zhou, K. Sun, and X. Mao, Nat. Commun. **8**, 14201 (2017).
[63] J. C. Maxwell, London, Edinburgh Dublin Philos. Mag. J. Sci. **27**, 250 (1864).
[64] L. Cremona, *Two Treatises on the Graphical Calculus and Reciprocal Figures in Graphical Statics* (Clarendon, Oxford, UK, 1890).
[65] M. J. Lawler, Phys. Rev. B **94**, 165101 (2016).
[66] N. Jia, C. Owens, A. Sommer, D. Schuster, and J. Simon, Phys. Rev. X **5**, 021031 (2015).
[67] V. V. Albert, L. I. Glazman, and L. Jiang, Phys. Rev. Lett. **114**, 173902 (2015).
[68] S. McHugh, Phys. Rev. Appl. **6**, 014008 (2016).
[69] A. S. Meeussen, J. Paulose, and V. Vitelli, Phys. Rev. X **6**, 041029 (2016).
[70] B. G.-g. Chen, N. Upadhyaya, and V. Vitelli, Proc. Natl. Acad. Sci. U.S.A. **111**, 13004 (2014).
[71] K. Roychowdhury and M. J. Lawler, Phys. Rev. B **98**, 094432 (2018).
[72] H. Flanders, *Differential Forms with Applications to the Physical Sciences* (Elsevier, Amsterdam, 1963), Vol. 11.
[73] J. P. D'Angelo, *Several Complex Variables and the Geometry of Real Hypersurfaces*, Studies in Advanced Mathematics Vol. 8 (CRC Press, Boca Raton, FL, 1993).